Composition, geometry and polarization influences on spectroscopic properties of Yb-doped LLnB (Ln= Y, Gd) monoclinic crystals

Marie Chavoutier, Hassan Ajrouche, Yannick Petit, Alain Garcia, Philippe Veber, Alexandre Fargues, Oudomsack Viraphong, Veronique Jubera, Inka Manek-Hönninger, Patricia Segonds, et al.

Composition, geometry and polarization influences on spectroscopic properties of Yb-doped LLnB (Ln= Y, Gd) monoclinic crystals.

Marie Chavoutier,[a,b] Hassan Ajrouche, [a,b] Yannick Petit, [a,b,c] Alain Garcia, [a,b] Philippe Veber, [a,b] Alexandre Fargues, [a,b] Oudomsack Viraphong, [a,b] Veronique Jubera,[a,b] Inka Manek-Hönninger,[c] Patricia Segonds,[d,e] Jérôme Debray, [d,e] Bertrand Menaert, [d,e] and Vincent Rodriguez,[f] Frédéric Adamietz,[f]

[a] CNRS, ICMCB, UPR 9048, F-33600 Pessac, France
[b] Univ. Bordeaux, ICMCB, UPR 9048, F-33600 Pessac, France
[c] LOMA (UMR 5798), CNRS, Université Bordeaux 1, 351 cours de la Libération, Talence Cedex, F-33405, France
[d] CNRS, Inst NEEL, F-38042 Grenoble, France
[e] Univ. Grenoble Alpes, Inst NEEL, F-38042 Grenoble, France
[f] Institut des Sciences Moléculaires (UMR 5255) CNRS, Université de Bordeaux, 351 cours de la Libération, Talence Cedex, F-33405, France

ABSTRACT

Characterizations of linear spectroscopic properties in polarized light have been performed for the highly-concentrated Yb-doped borate family $Li_6Ln(BO_3)_3$ (with Ln: Gd, Y, and labeled Yb:LLnB), in order to start to evaluate their potentiality for high-power laser applications. Modifications in spectral distributions and intensities are reported with respect to crystal orientation and polarization. Chemical composition and crystal shaping are discussed, pointing strong possible dependence with experimental conditions, which has to be considered so as to take sufficient precautions regarding the prediction of potential laser properties in such anisotropic laser crystals.

Keywords: borate, ytterbium, spectroscopic properties, laser crystals, crystal optics.

1- INTRODUCTION

Borates are interesting materials for laser applications thanks to their high damage threshold and their high transparency in the UV range. For spectroscopic aspects, ytterbium ions show advantages like a simple energy level diagram with no cross-relaxation process or excited-state absorption, a long lifetime and a broad emission compared to neodymium or thulium. Moreover, the small quantum defect between the pumping and lasing wavelengths makes this material attractive for its high efficiency and limited thermal effects. Thus laser systems based on ytterbium-doped materials have raised much interest since the development of powerful InGaAs diodes, for compact, high-power all-solid-state lasers.

In this context, the LYB:Yb ($Li_6Y(BO_3)_3:Yb^{3+}$) crystal has already proven interesting results for laser applications [1][3], as well as the whole solid solution LYB:Yb-LGB:Yb ($Li_6Y(BO_3)_3:Yb^{3+}$-$Li_6Gd(BO_3)_3:Yb^{3+}$) [4], depicting the crystal growth, and thermal, mechanical and optical properties. No polarized light study had been done, since measurements had been performed on powders (crushed single crystals). Since recent studies had reported monoclinic specificities of spectroscopic properties [5],[6], it was of interest to study our oriented LiLnB:Yb crystals in polarized light.

In this article, some absorption and emission cross-sections were recorded in polarized light in Yb(22%)-doped LLnB oriented cubes (chemical composition $Li_6Ln(BO_3)_3$, with Ln = Y, Gd). Related laser gain cross-sections were calculated and lifetime was measured. We also determined values of the three principal refractive indexes of these biaxial crystals. These results emphasize the potential of Yb-doped LYB-LGdB monoclinic crystals as candidates for laser applications.

2- EXPERIMENTAL RESULTS AND DISCUSSION

2.1 Crystallographic frame versus dielectric frame in monoclinic crystals

The linear optical properties are governed by the linear dielectric constant ε, depicted by a complex second-rank polar tensor. The real part of ε is related to the refraction properties, and it is diagonal in the orthonormal dielectric frame labeled (X, Y, Z) [7]. In the case of monoclinic crystals, the dielectric frame is linked only to one axis of the crystallographic frame (a, b, c), namely this monoclinic special axis. The two other axes of the orthonormal dielectric frame cannot be the a- and c-axis respectively since the crystallographic frame is not orthogonal. By convention the special axis is chosen as the b-axis, and the oriented angle (a, c) labeled β is typically close to 105° in our crystals [8]. In our crystals, we determined that the dielectric axis being linked to b-axis of the crystallographic frame is Y//b. This showed the absence of dispersion of the relative orientation between the crystallographic and the dielectric frames.

2.2 Orientation of the dielectric frame as a function of the wavelength in our crystals

Four crystals of LGB:Yb, $LG_{¾}Y_{¼}B$:Yb, $LG_{1/2}Y_{1/2}B$:Yb and $LG_{¼}Y_{¾}B$:Yb were grown with the ytterbium concentration of about 22% of atomic substitution of the rare earth element. Such Yb^{3+} concentrations in these new growth materials were checked by ICP chemical analysis. The relative proportion between yttrium and gadolinium ions is indicated as an index in the LLnB formula. These materials were compared to LYB:Yb (26%Yb-content) previously grown [3]. These crystals were cut as two oriented samples with faces polished to optical quality: one slab with two parallel faces oriented perpendicularly to the b-axis (b-cut slab), and one cube with all faces oriented perpendicularly to the three dielectric axes (Fig. 1). The LYB:Yb sample was just available as a b-cut slab. The orientation of the crystallographic b-axis, was determined with an accuracy of 0.25° by X-ray diffraction using the Laue method, and the dimensions of the oriented slabs were $1\times1\times0.09\ cm^3$. For the cubes, the same method was performed for the crystallographic orientation. Transmission conoscopy was necessary to obtain the complete dielectric orientation. It was performed at λ = 589 nm for two different crystal orientations, and the related interference patterns showed axes of symmetry that correspond to two axes of the dielectric frame (X, Y, Z) [9] (Fig. 1a and 1b for $LG_{¼}Y_{¾}B$:Yb crystal). Note that interference patterns are different in Fig. 1a and Fig. 1b, since Fig. 2b showed two "eyes" that correspond to the signature of the two optical axes of the index surface. By considering all our crystals from the positive biaxial optical class [10], the two polished faces of the slab depicted in Fig. 1a were then perpendicular to Z-axis of the dielectric frame and include b-axis that is colinear to Y-axis, and X-axis. The two polished faces in Fig. 1b were perpendicular to b = Y-axis, and include X- and Z- axis. Finally, the combination of X-Rays and conoscopy in all crystals led to the relative orientation between the crystallographic frame and the dielectric frame at 589 nm. Such relative orientation by α = (X, a) or γ = (Z, c) are linked by the relation $\alpha(\lambda) + \beta = 90° + \gamma(\lambda)$, as reported in Table 1 for LGB:Yb, $LG_{¾}Y_{¼}B$:Yb, $LG_{1/2}Y_{1/2}B$:Yb and $LG_{¼}Y_{¾}B$:Yb. They are negative values since the orientation of α-angle (Fig. 1c). If they slightly depend on the crystal composition, they are completely different from $Li_6Gd(BO_3)_3$: Nd^{3+} where α =9.7° (and γ = 5.7°) at 633 nm [10].

The orientation between the crystallographic and dielectric frames versus wavelength was checked by setting the cubes between crossed polarisers. The propagation direction was along b, and the X- and Z-axes were oriented along the polarizer axes to get a total extinction. The transmitted light was recorded between 720 and 1100 nm. The extinction maintained total, showing a constant dielectric frame orientation in this spectral range with an accuracy of 0.5°.

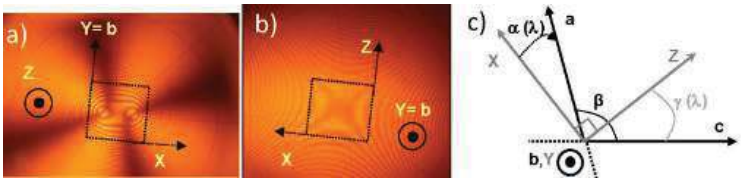

Figure 1- Transmission conoscopy interference patterns at 589 nm for a $LG_{¼}Y_{¾}B$:Yb crystal cut with two polished faces a) including the b-axis, b) perpendicular to the b-axis. The symmetry axes correspond to the dielectric axes. c) Orientation between the crystallographic frame and the dielectric frame, where $\alpha(\lambda) = (X, a)$, $\gamma(\lambda) = (Z, c)$ and $\alpha(\lambda) + \beta = 90° + \gamma(\lambda)$.

Table 1: α = (X, a) values determined by combining X-Rays and conoscopy at 589 nm

Crystal composition	LGB:Yb	$LG_{3/4}Y_{1/4}B$:Yb	$LG_{1/2}Y_{1/2}B$:Yb	$LG_{1/4}Y_{3/4}B$:Yb
α (+/- 0.5°)	-39.4°	-40.6°	-38.5°	-38.8°

2.3 Refractive index measurements

From X-ray diffraction combined to conoscopy, we were able to orientate cubes with their six faces polished to optical quality, and oriented perpendicularly to each of the three dielectric axes. The three principal refractive indices, n_x, n_y and n_z, of all the compositions were determined at 405 nm, by using an original Brewster method described elsewhere [11],[12]. No significant difference was obtained between the four gadolinium content materials, and thus we report here results on the LGB:Yb crystal. Refined values in LGB:Yb are equal to $n_x = 1.541$, $n_y = 1.568$ and $n_z = 1.572$. Associated Fresnel losses on the input samples are weak enough, and laser tests can be performed on crystals without coating: reflexion coefficients of intensities in normal incidence are between 4 % and 5.5 % per polished face in the visible. Note that the n_y value is the intermediate value, despite the mono-dimensional crystal structure, with LnO_8 polyhedra chains defined by the (a-c) planes, thus perpendicular to the b=Y-axis.

2.4 Linear spectroscopic characterizations

The linear spectroscopic characterization in polarized light was performed at 298 K, with a tuneable light source between 850 and 1050 nm through LGB:Yb, $LG_{¾}Y_{¼}B$:Yb, $LG_{1/2}Y_{1/2}B$:Yb, $LG_{¼}Y_{¾}B$:Yb and LYB:Yb b-cut slabs of 0.9 mm thickness. Absorption spectra were recorded on a Cary 5000, Varian instrument with polarized excitation. All fluorescence measurements were performed on a Fluorolog 3 Horiba with polarized collection and equipped with an InGaAs detector and using a polarized commercial laser diode. This led to the measurement of absorption and emission main cross-sections for the polarization eigenmodes, namely along the X- and Z-axes here.

2.4.1 Absorption cross-section

The absorption cross-section in polarized light is determined from the experimental transmission spectra, T(λ), versus wavelength as $\sigma_{abs}(\lambda) = -\ln\{T(\lambda)\}/(Nl) = \alpha(\lambda)/N$, where N is the ytterbium doping ions concentration (cm^{-3}), l (cm) the crystal length, and $\alpha(\lambda)$ (cm^{-1}) the measured absorption coefficient. The corresponding spectral distributions are illustrated in Fig. 2a and 2b for all the studied crystals, where the polarization is along X-axis and Z-axis, respectively.

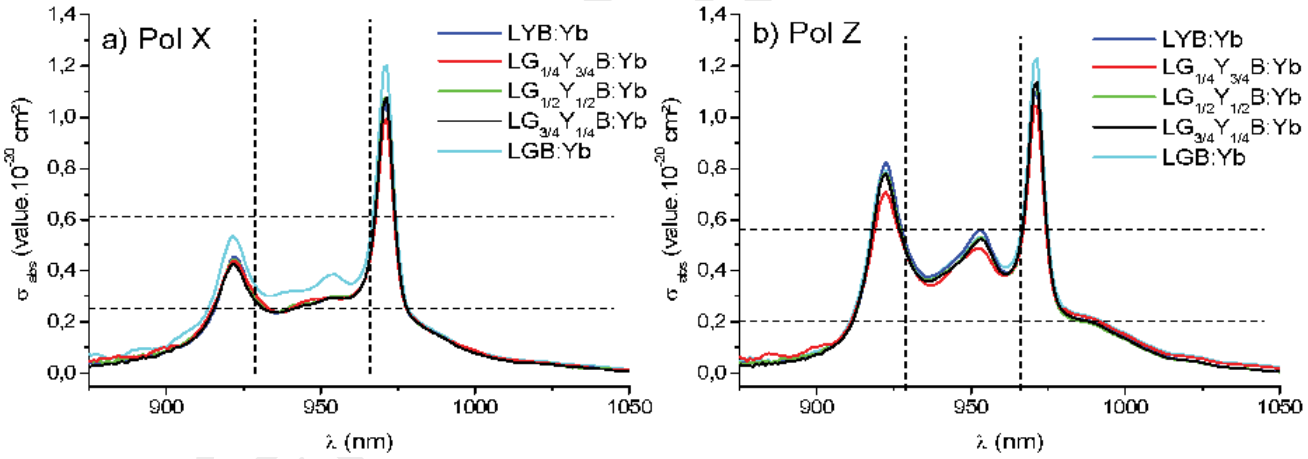

Figure 2- Absorption cross-sections in polarized light of b-cut Yb-doped L*Ln*B single crystal slabs (22% and 26% molar substitutions of the Gd-content crystal and the pure Y matrix, respectively) at 298 K: a) X-polarization, b) Z-polarization.

The whole solid solution's composition led to very similar spectral absorption distributions. However, a significant modification in the relative intensity can be distinguished between the X- and Z-polarization in the 930 - 960 nm spectral range. Also, the absorption cross-sections corresponding to the 1→7 and 1→6 transitions are both typically multiplied per two (915 – 960 nm spectral range). However, no difference is observed for the 1→5 transition, commonly used for pumping in a laser cavity. The weaker concentration of Gd-content crystal compared to the yttrium pure matrix does not result in a significant modification of the absorption cross-section.

2.4.2 Emission cross-section

The knowledge of the energy splitting of the Stark components makes possible the use of the reciprocity method to evaluate the emission cross-sections in polarized light [13]. Thus, emission cross-sections in polarized light were calculated from the measured absorption cross-sections, (Fig. 3a and 3b for b-cut slabs for the five LLn:Yb samples, plus a LYB:Yb sample), where polarizations were along the X- and Z-axis, respectively. A more efficient emission cross-

section is reported for the Z-polarization, with up to a 66% enhancement around 1 µm in the 980-1025nm range. If considering the laser emission wavelength previously reported on a yttrium matrix [1,2], a light improvement is seen for the X-polarization at 1040 nm, the highest value being attributed to the LGB:Yb composition.

The validity of the reciprocity method is mostly restrained to the higher energy components like the $^2F_{5/2}$ excited levels. Therefore, we have also collected emission spectra in polarized light with cubes having their six faces oriented perpendicularly to the three principal axes of the dielectric frame. The fluorescence at $\lambda_{em(Fluo)}$ was excited at λ_{exc} = 932 nm (in the 1→6 transition) with a linearly polarized commercial laser diode that successively propagated along each of the three dielectric axes. Fluorescence was collected in polarized light perpendicularly to the propagation direction of the pump, along another dielectric axis. The divergences of the excitation beam and of the collected fluorescence emission were estimated typically to ±1° and ±5°, respectively, ensuring a rather relevant angular resolution in the case of these low-symmetry crystals [14]. Fig. 4 shows an illustration of the experimental configuration, in the case where the diode is propagating along the Y-axis with a polarization along the Z-axis, while the emission is collected along the X-axis with a polarization along the Z-axis. Successively, a total of twenty four possible configurations were studied for each composition. Emission cross-sections were re-calculated by using the Füchtbauer-Ladenburg (FL) method [15], with the radiative lifetime measured on a crushed single crystal powder (table 3).

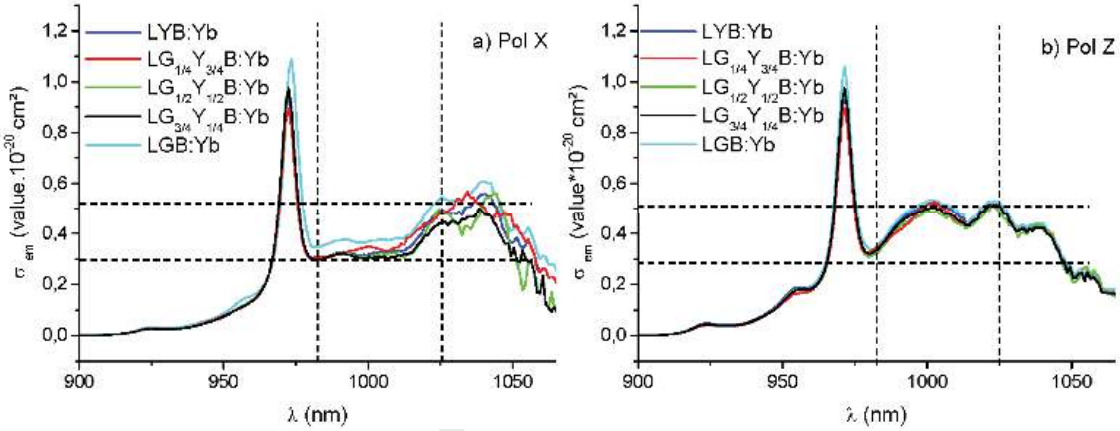

Figure 3- Emission cross-sections in polarized light along a b-cut Yb-doped L*Ln*B single crystal, calculated by the reciprocity method: a) X-polarization, b) Z-polarization.

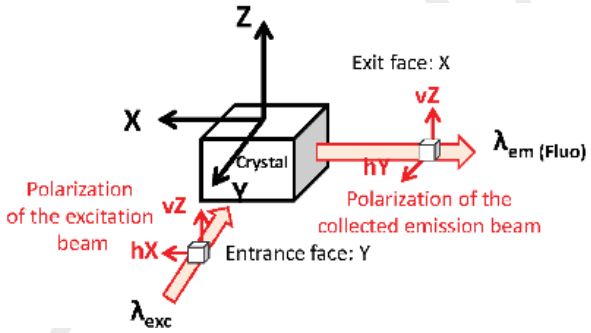

Figure 4- Example of orientation of the excitation and emission collection in polarized light among the twenty four possible for emission cross-section studies: these configurations correspond to 4 cases, among which one can be labelled FYhX-FXhY, corresponding to a pump propagation along the entrance face Y (FY), with a horizontal polarization parallel to the X-axis (hX), and associated to a fluorescence collection along the exit face X (FX), with a horizontal polarization parallel to the Y-axis (hX).

Emission cross-sections had previously been obtained with the reciprocity method with b-cut slabs (Fig. 3). Since these estimations did not show great differences among the five compositions, we focused on the $LG_{3/4}Y_{1/4}B$:Yb crystal. The associated sample dimensions reflect the geometry contribution to the collected data (Fig. 5). The fluorescence spectra are gathered in three graphs (Fig. 5a, 5b and 5c), according to the polarization of the collected luminescent beam along each dielectric axis, respectively. A superposition of three curves for one fixed excitation polarization, for each emission polarization along the three dielectric axes, is reported for comparison in Fig. 5d.

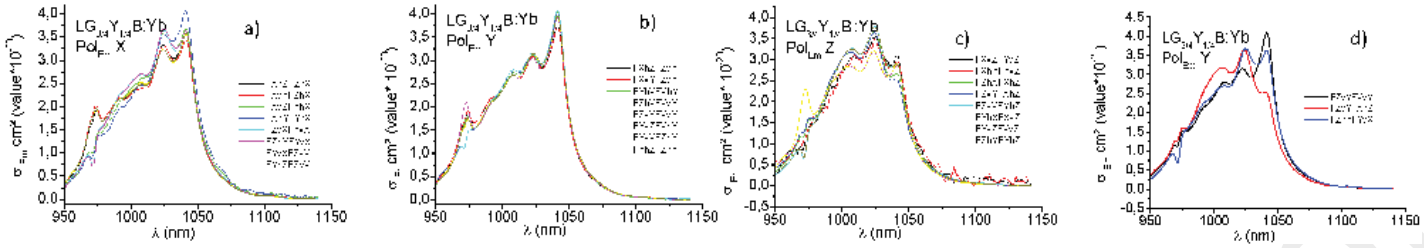

Figure 5- Emission cross-sections of a $LG_{3/4}Y_{1/4}B$:Yb oriented cube at 298 K, calculated by the FL method: a) X-polarized emission, b) Y- polarized emission, c) Z- polarized emission, d) Y-polarized excitation.
(legend explanation: FXhZ-FZhX = pump propagation perpendicularly to entrance face X (FX), with a horizontal polarization (hZ), while the collected fluorescence propagates along the exit face (FZ), with a horizontal polarization (hX).

The analysis of the collected results puts in evidence that the emitted spectral distribution is mainly run by the selected fluorescence polarization. Indeed, the directions of propagation and polarization of the excitation beam only impact the global intensity of the collected fluorescent emissions, but not their spectral distributions. Moreover, we also notice the strong influence of the re-absorption of the emission of the 5→1 transition, as seen on the relative intensity of the corresponding lines around 970 nm, showing an experimental influence of the optical path that fluorescence propagates to go out of the crystal, in close relation to the crystal dimensions. In some conditions, this phenomenon is so predominant that the 5→1 line appears as a "negative" contribution compared to the fluorescence emission background, as shown in each part of Fig. 5 around 970 nm. One can note, as observed on Fig. 3 (emission cross-section calculated from the absorption measurements with the same materials), a maximal emission efficiency around 1020 nm and at 1040 nm for the fluorescence polarization along the Z- and X-axis, respectively. The third polarization direction (along the Y-axis) shows that the Y-polarization is also maximal at 1040 nm. One observes that the preponderant re-absorption process according for the 5→1 transition leads to significant spectral distortions and to an artificial increase of the emission cross-section at higher wavelengths. Spectral normalization of fluorescence spectra with the FL method is thus affected, leading to a mismatch of absolute amplitudes of the emission cross-sections at low energy, explaining the strong difference of emission cross-sections obtained with the reciprocity and FL methods. Despite these considerations, it appears instructive to reveal the emission anisotropy along the three principal axes of the dielectric frame.

2.4.3 Lifetime measurements

Lifetime measurements may also experimentally be be affected by the sample geometry. Decay times were measured both on crushed micrometric powder crystals and bulky oriented cubes of the $LG_{¾}Y_{¼}B$:Yb composition, showing the influence of the re-absorption process. The fluorescence lifetime of the excited state was recorded (oscilloscope LeCroy Waverunner LT 342, with a germanium AD 403HS detector coupled to a monochromator CVI R110). The excitation source was a commercial fibre-coupled laser diode controlled by a function generator (HM 8030), delivering a TTL square signal at 10 Hz. Two excitation wavelengths coupled with two or three emission lines were observed. Decay profiles were correctly fitted with a single exponential decay. Results obtained for $LG_{¾}Y_{¼}B$:Yb are listed on Table 3.

Table 3: Lifetime measurements in milliseconds

$LG_{¾}Y_{¼}B$:Yb	λ_{em}	λ_{exc}= 940 nm	λ_{exc}= 985 nm
Crushed crystals	975 nm	1.110	-
	1030 nm	1.154	1.147
	1040 nm	1.160	1.147
Oriented cubes	975 nm	-	-
	1030 nm	1.523	1.472
	1040 nm	1.521	1.482

With powders, a weak evolution of a few percents of the decay time value can be noticed for an excitation at 940 nm. Such variation is not detected anymore for a 985 nm excitation, suggesting the experimental resolution of the setup and the distinct ability to filter the diode spectrum of the two considered cases. Moreover, a strong increase of the decay time is visible for the acquisitions with the oriented cubes, compared to crushed crystals. Such decay time lengthening reflects energy transfers from the higher energy component (5→1 line) to the lower ones. Also no visible emission due to cooperative emission from up-conversion processes from impurities [16] has been observed here. Thus, emission cross-sections were calculated with lifetime values from crushed crystals. Note that in a laser cavity pumped at 972 nm, the stimulated emission at 1030 nm occurs much faster than the fluorescence lifetime, cancelling thus such effect of lifetime lengthening. Finally, measurements confirm that there is one single fluorescence lifetime for the excited Yb^{3+} ions.

2.4.4 Calculated gain cross-section

Laser gain cross-sections were calculated as $\sigma_{gain}(\lambda) = \beta\sigma_{em}(\lambda)-(1-\beta)\sigma_{abs}(\lambda)$, with $\beta = N_2/N_1$ the population inversion rate. We used absorption cross-sections (σ_{abs}) from the absorption spectra with the b-cut slabs, and the related emission cross-sections (σ_{em}) from the reciprocity method. Since the absorption cross-sections of the five b-cut slabs were similar, only the $LG_{3/4}Y_{1/4}B$:Yb gain is showed in Fig. 6a and 6b for the X- and Z-polarization, respectively. Indeed, the gain cross-sections are polarization-dependent. Except the 5→1 line, the highest gain cross-section (0.5×10^{-20} cm^2) was obtained for the X-polarization at 1040 nm. The Z-polarization showed a larger range with homogeneous gain range around 990-1040 nm, which is interest for ultra-short pulse generation. Since this method misrepresents re-absorption effects, the calculated cross-sections appear higher than for other borates [17][18].

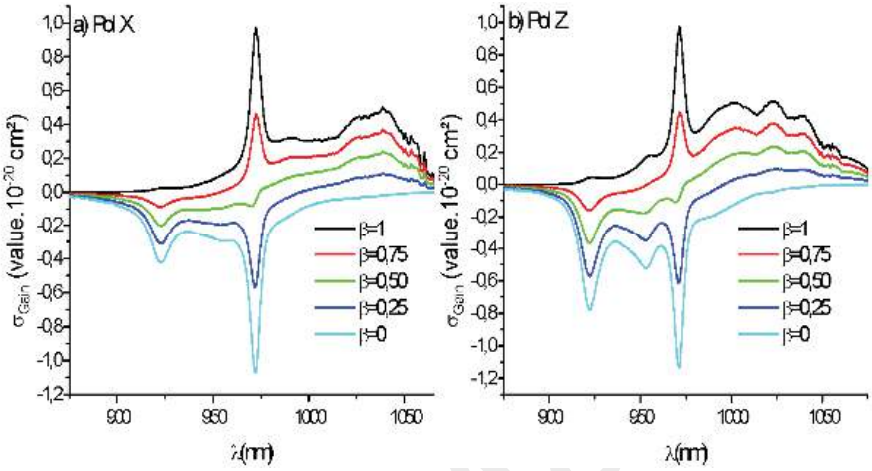

Figure 6- Laser gain cross-section calculation from the reciprocity method for a $LG_{3/4}Y_{1/4}B$:Yb b-cut slab: a) X- and b) Z-polarization.

Table 2- Absorption and emission cross-sections in polarized light.

value×10^{-20} cm^2		$\sigma_{abs}^{\lambda pump}$	$\sigma_{abs}^{\lambda laser}$	$\sigma_{em}^{\lambda pump}$	$\sigma_{em}^{\lambda laser}$
$LG_{3/4}Y_{1/4}B$:Yb	X-polarization	1.58	0.02	1.46	0.5
	Z-polarization	1.67	0.01	1.54	0.36

3- CONCLUSION

This study reports on the preliminary spectroscopic characterizations in polarized light of the high optical quality Yb-doped family of LLnB materials (chemical formula: $Li_6Ln(BO_3)_3$, with Ln: Gd, Y), to evaluate their potentiality for high-power laser applications. Absorption, fluorescence emission and laser gain cross-sections were measured in polarized light. This work shows that the doping element concentration and the crystal sample geometries represent two major criteria to characterize absorption and emission processes. Surprisingly, with respect to previous spectroscopic measurements with powders [4], the relative ratio between yttrium and gadolinium has no impact on the observed data. Furthermore, no modification of the spectral distribution of the absorption and emission cross-sections is observed for this solid solution family. For this reason, we mainly focused on results of the monoclinic $LG_{3/4}Y_{1/4}B$:Yb compound.

This work is based on the crystal orientation with respect to the direction of propagation and the polarization orientation with respect to the three main axes of the dielectric frame. As expected for a monoclinic crystal, it clearly shows a significant anisotropy of absorption and emission properties. The absorption cross-section of the 1→5 transition seems to be equivalent whatever the polarization whereas the X- and Z-polarization show a significant difference for the 1→6 and 1→7 lines, which should be considered when choosing the pumping wavelength for future laser tests. For emission, a maximum is observed for the X-polarization. Additionally, these highly-doped materials evidenced strong re-absorption effects, in relation to their geometrical aspects, requiring caution for interpretation.

Finally, we expect that interesting laser performances of these borate compounds can be obtained and improved, especially by an optimized crystal orientation in the monoclinic plane. Still, the broadband fluorescence emission makes these Yb-doped $LY_{1-x}Gd_xB$ ($0<x<1$) crystals as good candidates for ultrafast laser applications.

ACKNOWLEDGMENTS

The work was funded by Conseil Régional d'Aquitaine (N°20071101024, PhD of M. Chavoutier), CNRS and GIS AMA (LasINOF Univ. Bordeaux).

REFERENCES

[1] J. Sablayrolles, V. Jubera, J.P. Chaminade, I. Manek-Hönninger, S. Murugan, T. Cardinal, R. Olazcuaga, A. Garcia, F. Salin, Opt. Mater. (Amsterdam, Neth.) **27,** 1681-1685 (2005).

[2] M. Delaigue, V. Jubera, J. Sablayrolles, J.-P. Chaminade, A. Garcia, I. Manek-Hönninger, Appl. Phys. B: Lasers Opt. **87(4),** 693–696 (2007).

[3] J. Sablayrolles, V. Jubera, M. Delaigue, I. Manek-Hönninger, J-P. Chaminade, J.Hejtmanek, R. Decourt, A. Garcia, Mater. Chem. Phys. **115,** 512–515 (2009).

[4] M. Chavoutier, V. Jubera, P. Veber, I. Manek-Hönninger, D. Descamps, A. Garcia, O. Viraphong, J. Hejtmanek, R. Decourt, B. Menaert, F. Adamietz, V. Rodriguez, A. Fargues, F. Guillen, M. Velazquez, J Solid State Chem. **184(2),** 441–446 (2011).

[5] Y. Petit, B. Boulanger, P. Segonds, C. Félix, B. Ménaert, J. Zaccaro, G. Aka, Opt. Expr. **16,** 7997-8002 (2008).

[6] Y. Petit, S. Joly, P. Segonds, B. Boulanger, Laser & Photon. Rev. **1-18** (2013) DOI 10.1002/lpor.201200078

[7] Born & Wolf, Principles of Optics, Oxford Pergamon press (1965).

[8] M . Chavoutier, University of Bordeaux PhD, (2010) n° 4091.

[9] A. N. Winchell "Elements of Optical mineralogy, Part I Principles and Methods", John Wiley & Sons Inc. 5th ed., New York USA (1965).

[10] X. Gong, Y. Lin, Y. Chen, Z. Luo, Q. Tan, Y. Huang J. Opt. Soc. Am. B **23(10)**, 2059-2065 (2006).

[11] V. Rodriguez, C. Sourisseau, J. Opt. Soc. Am. B **19**, 2650–2664 (2002).

[12] V. Rodriguez, J. Chem. Phys. **128(6)**, 064707-064716 (2008).

[13] D. E. McCumber, Phys. Rev. A **136(4),** 954-957 (1964).

[14] Y. Petit, S. Joly, P. Segonds, B. Boulanger, Laser Physics **21**, 1305-1312 (2011).

[15] P. F. Moulton, J. Opt. Soc. Am. B **3**, 125-133 (1986).

[16] E. Nakazawa and S. Shionoya, Phy. Rev. Lett. **25(25)**, 1710-1712 (1970).

[17] V. Jubera, P. Veber, M. Chavoutier, A. Garcia, F. Adamietz, V. Rodriguez, J. Chaminade, M. Velazquez, CrystEngComm. **12**, 355-357 (2010).

[18] F. Augé, F. Balembois, P. Georges, A. Brun, F. Mougel, G. Aka, A. Kahn-Harari, D. Vivien, Appl. Opt. **38(6),** 976-979 (1999). A. Brenier and G. Boulon, Europhys. Lett. **55(5),** 647-652 (2001). S. Chénais, F. Druon, F. Balembois, P. Georges, R. Gaumé, P. H. Haumesser, B. Viana, G. Aka, D. Vivien, J. Opt. Soc. Am. B **19**, 1083-1091 (2002).